

MnCo₂S₄/CoS₂ Electrode for Ultrahigh Areal Capacitance

Rahul B. Pujari¹, C. D. Lokhande², and Dong-Weon Lee^{1,*}

Abstract

MnCo₂S₄/CoS₂ electrode with highly accessible electroactive sites is prepared using the hydrothermal method. The electrode exhibits an areal capacitance of 0.75 Fcm⁻² at 6 mAc⁻² in 1 M KOH. The capacitance is further increased to 2.06 Fcm⁻² by adding K₃Fe(CN)₆ and K₄Fe(CN)₆ (a redox couple) to KOH. This increment is associated with the redox-active properties of cobalt and manganese transition metals, as well as the ion pair of [Fe(CN)₆]³⁻/[Fe(CN)₆]⁴⁻. The capacitance retention of the MnCo₂S₄/CoS₂ electrode is 87.5% for successive 4000 charge–discharge cycles at 10 mAc⁻² in a composite electrolyte system of KOH and ferri/ferrocyanide. The capacitance enhancement is supported by the lowest equivalent series resistance (0.62 Ωcm⁻²) of MnCo₂S₄/CoS₂ in the presence of redox additive couple compared with the bare KOH electrolyte.

Keywords: Hydrothermal, CoS₂, MnCo₂S₄, Redox additive, Supercapacitor

1. INTRODUCTION

Supercapacitors, unlike electrostatic capacitors, are endowed with moderate energy density and high power density [1]. Energy density is directly related to capacitance, i.e., $E = 0.5CV^2$. Out of various ways to improve the capacitance of supercapacitors, electrodes based on transition metals, e.g., MnO₂ [2] and MoO₃ [3], are very effective than carbon-derived materials. Recently, transition metal sulfides are intensively tested like CoS₂ [4] owing to the superiority of electrically conductive nature compared with the oxide electrodes. Even bimetallic sulfide electrodes, such as NiCo₂S₄ [5], Zn_{0.76}Co_{0.24}S [6], CuCo₂S₄ [7], MnCo₂S₄ [8] and M_xCo_{3-x}S₄ (M = Ni, Mn, Zn) [9], cannot improve the targeted energy storage for supercapacitor devices. It is anticipated that the composite electrode of the MnCo₂S₄ and CoS₂ will achieve targeted capacitance and energy density of supercapacitor. The individual redox activities of MnCo₂S₄ and CoS₂ as well as electrochemical interactions between them will enhance

performance of the composite electrode.

Furthermore, the practices have been done to improve the capacitance of aqueous supercapacitors using redox additives in parent electrolytes, e.g., K₃Fe(CN)₆. Previously, the capacitance of the graphene paper electrode was enhanced to 475 mFcm⁻² from 93 mFcm⁻² (obtained from the bare Na₂SO₄ electrolyte) using the K₃Fe(CN)₆/Na₂SO₄ redox electrolyte system [10]. Moreover, capacitance improvement has been observed in Co–Al–layered double hydroxide [11] and Co(OH)₂ [12] by pouring K₃Fe(CN)₆ or K₄Fe(CN)₆ into 1 M KOH.

However, the hydrothermal synthesis of the MnCo₂S₄/CoS₂ electrode and its electrochemical charge storage performance are yet to be explored in a redox-active electrolyte. Therefore, we have prepared a highly accessible MnCo₂S₄/CoS₂ electrode using the hydrothermal method, and its electrochemical charge storage is evaluated in 1 M KOH electrolyte. The capacitance increment of the MnCo₂S₄/CoS₂ electrode is more than two times in the redox active electrolyte compared with bare KOH.

2. EXPERIMENTAL DETAILS

2.1 Synthesis of MnCo₂S₄/CoS₂

Manganese sulfate (MnSO₄), cobalt sulfate (CoSO₄), thiourea (SC(NH₂)₂), and urea (CO(NH₂)₂) (Thomas Baker Pvt. Ltd., Mumbai) were used without further treatments. MnSO₄ (100 mM), CoSO₄ (200 mM), SC(NH₂)₂ (400 mM), and CO(NH₂)₂ (200 mM) were dissolved successively in 40 ml of double-distilled

¹MEMS and Nanotechnology Laboratory, School of Mechanical System Engineering, Chonnam National University, Gwangju, 61186, Republic of Korea,

²Centre for Interdisciplinary Research, D.Y. Patil Education Society (Deemed to be University), Kolhapur (M.S.), 416 006, India.

*Corresponding author: mems@jnu.ac.kr

(Received : May. 27, 2020, Revised : Jul. 23, 2020, Accepted : Jul. 29, 2020)

This is an Open Access article distributed under the terms of the Creative Commons Attribution Non-Commercial License (<https://creativecommons.org/licenses/by-nc/3.0/>) which permits unrestricted non-commercial use, distribution, and reproduction in any medium, provided the original work is properly cited.

water (DDW) under constant magnetic stirring to produce a final solution. Then, type 304 stainless steel (SS) substrate was polished using a zero-grade silicon carbide paper and cleaned with DDW. Then, the substrate was placed and aligned with the solution in a 40-ml glass beaker. The beaker was placed in a 16-L hydrothermal SS autoclave and heated at 363 K for 5 h. After the chemical reaction, the $\text{MnCo}_2\text{S}_4/\text{CoS}_2$ thin-film electrode of sky blue color was formed on the SS substrate. The electrode was removed from the autoclave and cleaned with DDW and ethanol.

2.2 Materials characterization

The growth orientation of material and crystal structure was analyzed with the Bruker X-ray diffractometer using the X-ray diffraction (XRD) technique. The chemical states of different elements present in the material were analyzed using the X-ray photoelectron spectroscopy (XPS) technique. The surface morphology of the thin film was assessed using field emission scanning electron microscopy (FE-SEM). The electrochemical charge storage of electrode was evaluated in 1 M KOH, 1 M KOH + 0.05 M $\text{K}_3\text{Fe}(\text{CN})_6$, and 1 M KOH + 0.025 M $\text{K}_3\text{Fe}(\text{CN})_6$ + 0.025 M $\text{K}_4\text{Fe}(\text{CN})_6$ electrolytes. The electrochemical impedance of $\text{MnCo}_2\text{S}_4/\text{CoS}_2$ was measured in the aforementioned electrolytes in the range of 0.1 Hz to 100 kHz with an AC amplitude of 10 mV and zero biased potential. Electrochemical measurements were performed using the ZIVE SP5 electrochemical workstation with three electrode cell comprising $\text{MnCo}_2\text{S}_4/\text{CoS}_2$, standard calomel, and platinum plate as working, reference, and counter electrodes, respectively.

3. RESULTS AND DISCUSSIONS

3.1 Physico-chemical study

The crystallinity of material plays a significant role in the performance of electrode materials; thus, the crystal structure and growth orientation of composite material is assessed based on the XRD pattern (Fig. 1). Highly intense XRD peaks of the electrode materials suggest that they are well crystallized. The XRD peaks indicated with (200), (210), (222), and (230) are associated with the CoS_2 phase of cobalt sulfide. The other peaks marked with (111), (220), and (222) should be considered for the MnCo_2S_4 phase of manganese cobalt sulfide [13]. Thus, the composite of the highly crystalline $\text{MnCo}_2\text{S}_4/\text{CoS}_2$ material is identified using XRD.

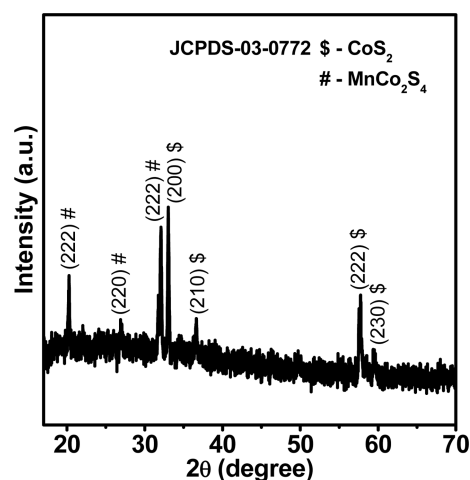


Fig. 1. (a) XRD pattern of $\text{MnCo}_2\text{S}_4/\text{CoS}_2$.

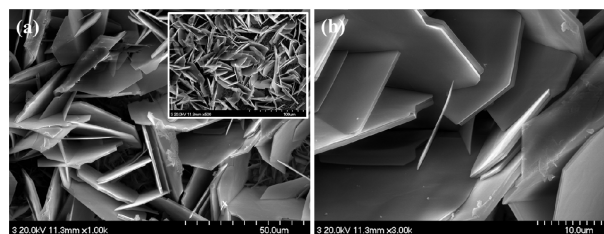


Fig. 2. (a, b) FE-SEM images of the $\text{MnCo}_2\text{S}_4/\text{CoS}_2$ electrode at different resolutions. The inset shows a low-resolution image.

The surface morphology of the electrode material mainly affects the electrochemical performance. The FE-SEM images of the $\text{MnCo}_2\text{S}_4/\text{CoS}_2$ electrode (Fig. 2a-b) show vertical interlocked discs at micro- to nanoscale, with incorporated large pores and vertical nanoflakes present underneath the discs. Such surface morphology is highly accessible for electrolyte ions during the electrochemical performance and extremely useful for supercapacitor applications. The discs and nanoflakes are connected to their side edges, which can tolerate high-rate charging and discharging during electrochemical interactions with electrolyte ions. The porous microstructure surface material facilitates easy ion intercalation and de-intercalation into an electrode matrix, which can improve charge kinetics in the material. Such discs and 2-D flakes help reduce electron transfer with successive nanodiscs during the electrochemical performance.

3.2 Electrochemical study

Cyclic voltammetry (CV) is a fundamental technique for analyzing charge storage kinetics in a material. The CV curves of the $\text{MnCo}_2\text{S}_4/\text{CoS}_2$ are measured at scan rates of 5–100 mVs^{-1}

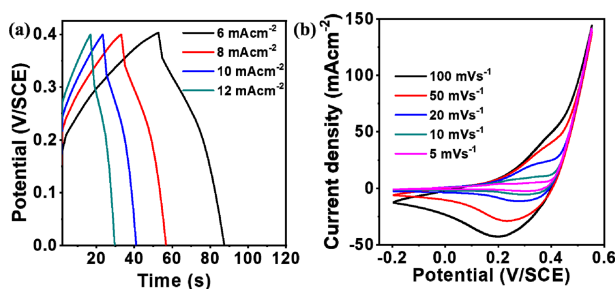


Fig. 3. (a) CV curves at scan rates of 5–100 mVs⁻¹. (b) GCD curves at 6–12 mAcm⁻² of MnCo₂S₄/CoS₂ in the KOH electrolyte.

within -0.2 to + 0.55 V/SCE potential window, initially in 1 M KOH electrolyte and then in redox active electrolytes, i.e., 0.05 M K₃Fe(CN)₆ + 1 M KOH and 0.025 M K₃Fe(CN)₆ + 0.025 M K₄Fe(CN)₆ + 1 M KOH. For convenience, 0.05 M K₃Fe(CN)₆ + 1 M KOH and 0.025 M K₃Fe(CN)₆ + 0.025 M K₄Fe(CN)₆ + 1 M KOH electrolytes are referred to as K₃KOH and K₃K₄KOH, respectively. The CV curves of MnCo₂S₄/CoS₂ electrode in the KOH electrolyte (Fig. 3a) show a shift in oxidation and reduction peaks toward high and low potential with increasing scan rate; this shift indicates the pseudocapacitive behavior of the electrode.

Similarly, it has occurred in the case of galvanostatic charge–discharge profile of the electrode at different current densities (Fig. 3b), which supports the CV analysis. The CV curves of MnCo₂S₄/CoS₂ (Fig. 4a) in K₃KOH demonstrates an increase in cathodic and anodic current densities owing to the presence of the redox-active K₃K₄KOH component, and the current density further increases in case of K₄Fe(CN)₆ and K₃K₄KOH electrolytes.

As compensating [Fe(CN)₆]³⁻ and [Fe(CN)₆]⁴⁻ ions are present in K₃K₄KOH, the symmetric CV curves of the electrode are seen for K₃K₄KOH than that for K₃KOH electrolyte. Moreover, the CV curves (Fig. 3a) in KOH exhibit a pair of reduction and oxidation peaks, while for K₃K₄KOH (Fig. 4a-b), an additional pair of reduction and oxidation peaks has been observed at each scan rate owing to the charge transfer between [Fe(CN)₆]³⁻ and [Fe(CN)₆]⁴⁻. The electronic exchange between KOH and MnCo₂S₄/CoS₂ is defined by the following reaction:



For the K₃KOH electrolyte, K₃Fe(CN)₆ molecules produce the ion pair of [Fe(CN)₆]³⁻/[Fe(CN)₆]⁴⁻, which adds pseudocapacitance, as shown in equation (2). In case of K₃K₄KOH, [Fe(CN)₆]³⁻ and [Fe(CN)₆]⁴⁻ are already present in the electrolyte in equal concentration; thus, symmetric CV curves are observed with increased current densities. Additional electron sharing between [Fe(CN)₆]³⁻ and [Fe(CN)₆]⁴⁻ during the charging and discharging

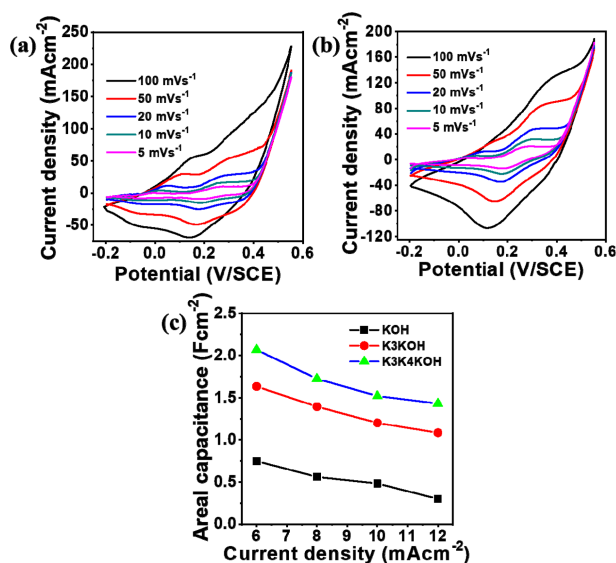


Fig. 4. CV curves of MnCo₂S₄/CoS₂ recorded in (a) K₃KOH and (b) K₃K₄KOH electrolytes. (c) Areal capacitances vs scan rate plot.

of the electrode in K₃K₄KOH (rather than in K₃KOH) is defined by the following reaction:



The areal capacitance (C_a) of the MnCo₂S₄/CoS₂ electrode in different electrolytes are calculated using the following equation:

$$C_a = \frac{v_1}{A \times v} \int_{v_1}^{v_2} I(V) dV \quad (3)$$

where the numerator part is the integral area of the CV curve for each scan rate (v) and A is the area (1 cm²) of the MnCo₂S₄/CoS₂ electrode. The v_1 and v_2 are the lowest negative and highest positive potentials, respectively, of the CV curves. The MnCo₂S₄/CoS₂ electrode has exhibited the highest capacitance of 2.4 Fcm⁻² at a scan rate of 5 mVs⁻¹ in the K₃K₄KOH electrolyte compared with the capacitance in KOH (0.8 Fcm⁻²; Fig. 4c). Thus, the capacitance increment of MnCo₂S₄/CoS₂ in K₃K₄KOH is attributed to pseudocapacitance of the redox activity of cobalt and manganese transition metals associated with the MnCo₂S₄/CoS₂ electrode materials, as well as the redox activity of [Fe(CN)₆]³⁻/[Fe(CN)₆]⁴⁻ present in the electrolyte solution. The decrease in the capacitance of the MnCo₂S₄/CoS₂ electrode is observed and attributed to charge transfer and mass transfer polarization at high scan rates [3, 4].

Moreover, the charge storage of MnCo₂S₄/CoS₂ is evaluated

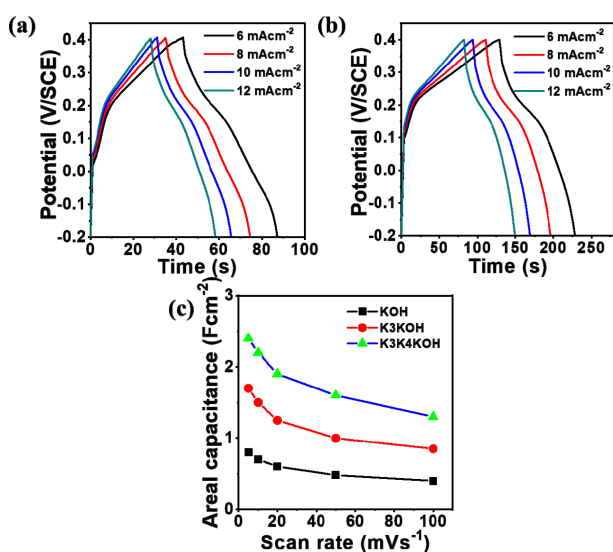


Fig. 5. GCD curves of MnCo_2S_4 at various current densities in (d) K_3KOH and (e) $\text{K}_3\text{K}_4\text{KOH}$ electrolytes. (f) Variation in areal capacitance of $\text{MnCo}_2\text{S}_4/\text{CoS}_2$ in different electrolytes.

based on the GCD measurements in the K_3KOH and $\text{K}_3\text{K}_4\text{KOH}$ electrolytes (Fig. 5a-c). The GCD curves at different current densities show non-linear shapes during the charging and discharging of the electrode suggesting the pseudocapacitive contribution of the material in addition to electrochemical double layer capacitance (EDLC) [3, 4]. In the GCD curves, the discharging part shows the initial potential drop caused by the internal resistance of the electrode material and the subsequent curved portion demonstrating the redox activity of the material. Increased electrochemical reactions, as shown by equation (2), and the presence of the ferri and ferrocyanide ion pair near to the electrode surface have pushed the charging and discharging time of $\text{MnCo}_2\text{S}_4/\text{CoS}_2$ to a higher scale in $\text{K}_3\text{K}_4\text{KOH}$. Therefore, the maximum areal capacitance of 2.06 Fcm^{-2} at a current density of 6 mAcm^{-2} is obtained in $\text{K}_3\text{K}_4\text{KOH}$ compared with 1.08 Fcm^{-2} in K_3KOH and 0.75 Fcm^{-2} in KOH (Fig. 5c). The obtained 2.06 Fcm^{-2} areal capacitance of the $\text{MnCo}_2\text{S}_4/\text{CoS}_2$ electrode is higher than recently reported 0.475 Fcm^{-2} for graphene paper electrode in redox active (Composite of $\text{K}_3\text{Fe}(\text{CN})_6$, $\text{K}_4\text{Fe}(\text{CN})_6$ and Na_2SO_4) electrolyte [9]. The cyclic lifetime of the $\text{MnCo}_2\text{S}_4/\text{CoS}_2$ electrode is evaluated in all three electrolytes for successive 4000 GCD cycles performed at 10 mAcm^{-2} . Fig. 6a shows capacitive retentions of 89%, 88%, and 87.5% of $\text{MnCo}_2\text{S}_4/\text{CoS}_2$ in KOH , K_3KOH , and $\text{K}_3\text{K}_4\text{KOH}$, respectively, after 4000 cycles demonstrating that cycling life of electrode is not influenced with addition of $\text{K}_3\text{Fe}(\text{CN})_6$ and $\text{K}_4\text{Fe}(\text{CN})_6$ redox additives. Thus, exhibits stable composite system of three different electrolytes.

The impedance of $\text{MnCo}_2\text{S}_4/\text{CoS}_2$ was measured to analyze

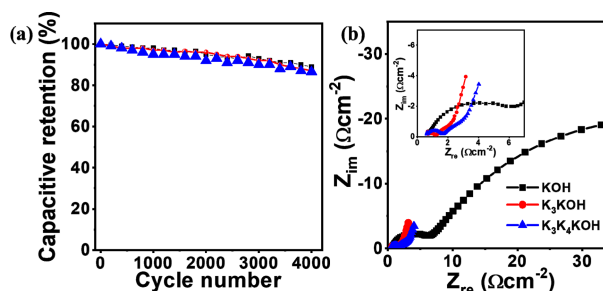


Fig. 6. (a) Capacitive retention of $\text{MnCo}_2\text{S}_4/\text{CoS}_2$ in KOH , K_3KOH , and $\text{K}_3\text{K}_4\text{KOH}$ electrolytes for 4000 GCD cycles measured at 10 mAcm^{-2} . (b) Nyquist curves of $\text{MnCo}_2\text{S}_4/\text{CoS}_2$ in various electrolytes measured at $0.1-10^5 \text{ Hz}$; the inset shows the magnified part of the Nyquist curves in high and mid-high frequency regions.

electrochemical reaction kinetics of the electrode in different electrolytes and calculate different resistances at the electrode–electrolyte interface. Fig. 6b shows the impedance spectra of $\text{MnCo}_2\text{S}_4/\text{CoS}_2$ in different electrolytes showing initial intersection with the real axis known to equivalent series resistance (ESR), which comprises electronic resistance and ionic resistance of the electrode–electrolyte system. The electronic resistance is caused by the intrinsic resistance of electrode material as well as resistance between electrode and current collector [13]. The ionic resistance is caused by movement of electrolyte ions in the electrolyte and the pores of the electrode material. The lowest ESR of $0.62 \text{ }\Omega/\text{cm}^2$ is obtained for $\text{MnCo}_2\text{S}_4/\text{CoS}_2$ in $\text{K}_3\text{K}_4\text{KOH}$ compared with that in K_3KOH and KOH (0.66 and $0.73 \text{ }\Omega/\text{cm}^2$, respectively). The lower ESR facilitates higher electronic and ionic transfer at the electrode–electrolyte interface in $\text{K}_3\text{K}_4\text{KOH}$, which assures maximum supercapacitive performance of the electrode.

4. CONCLUSIONS

The $\text{MnCo}_2\text{S}_4/\text{CoS}_2$ electrode has been prepared using a single-step hydrothermal method with the surface morphology similar to interconnected vertically aligned discs. The electrode exhibited excellent electrochemical charge storage of 0.75 Fcm^{-2} at 6 mAcm^{-2} in 1 M KOH owing to the redox activity of manganese and cobalt transition metals incorporated in the electrode materials. It is increased to 2.06 Fcm^{-2} in $\text{K}_3\text{K}_4\text{KOH}$ caused by the $[\text{Fe}(\text{CN})_6]^{3-}/[\text{Fe}(\text{CN})_6]^{4-}$ ion pair in the redox-active electrolyte. The cyclic lifetime of the $\text{MnCo}_2\text{S}_4/\text{CoS}_2$ electrode exhibited capacitance retention of 87.5% in redox active electrolyte, even after 4000 GCD cycles at 10 mAcm^{-2} , and it is not affected by the

[Fe(CN)₆]³⁻/[Fe(CN)₆]⁴⁻ ion pair, which shows the stability of the K₃K₄KOH electrolyte. The maximum pseudocapacitive charge storage of MnCo₂S₄/CoS₂ in K₃K₄KOH is supported by a decrease in ESR to 0.62 Ωcm⁻² compared with 0.73 Ωcm⁻² in the KOH electrolyte.

ACKNOWLEDGMENT

1. This study was supported by the National Research Foundation of Korea (NRF) under grant No. 2015R1A4A1041746 funded by the Korean Government (MSIP).

2. The authors are thankful to the Department of Science and Technology, Govt. of India, for financial support through the research project, Materials for Energy Storage, under sanction no. [DST/TMD/MES.2K17/04 (C&G)] dated July 17, 2018.

REFERENCES

- [1] T. Zhao, H. Jiang, and J. Ma, "Surfactant-assisted electrochemical deposition of a cobalt hydroxide for supercapacitors", *J. Power Sources*, Vol. 196, No. 2, pp. 860-864, 2011.
- [2] M. Huang, F. Li, F. Dong, Y. X. Zhang, and L. L. Zhang, "MnO₂-based nanostructures for high-performance supercapacitors", *J. Mater. Chem. A*, Vol. 3, No. 43, pp. 21380-21423, 2015.
- [3] R. B. Pujari, V. C. Lokhande, V. S. Kumbhar, N. R. Chodankar and C. D. Lokhande, "Hexagonal microrods architected MoO₃ thin film for supercapacitor application", *J. Mater. Sci.: Mater. Electron.*, Vol. 27, No. 4, pp. 3312-3317, 2016.
- [4] Y. Ji, X. Liu, W. Liu, Y. Wang, H. Zhang, M. Yang, X. Wang, X. Zhao, and S. Feng, "A facile template-free approach for the solid-phase synthesis of CoS₂ nanocrystals and their enhanced storage energy in supercapacitors", *RSC Adv.*, Vol. 4, No. 19, pp. 50220-50225, 2014.
- [5] W. Kong, C. Lu, W. Zhang, J. Pu, and Z. Wang, "Homogeneous core-shell NiCo₂S₄ nanostructures supported on nickel foam for supercapacitors", *J. Mater. Chem. A*, Vol. 3, No. 23, pp. 12452-12460, 2015.
- [6] Y. Liang, Q. Liu, Y. Luo, X. Sun, Y. He, and A. M. Asiri, "Zn_{0.76}Co_{0.24}S/CoS₂ nanowires array for efficient electrochemical splitting of water", *Electrochim. Acta*, Vol. 190, No. 1, pp. 360-364, 2016.
- [7] Q. Wang, X. Liang, D. Yang, and D. Zhang, "Facile synthesis of novel CuCo₂S₄ nanospheres for coaxial fiber supercapacitors", *RSC Adv.*, Vol. 7, No. 48, pp. 29933-29937, 2017.
- [8] A. M. Elshahawy, X. Li, H. Zhang, Y. Hu, K. H. Ho, C. Guan and J. Wang, "Controllable MnCo₂S₄ nanostructures for high performance hybrid supercapacitors", *J. Mater. Chem. A*, Vol. 5, No. 16, pp. 7494-7506, 2017.
- [9] Y. M. Chen, Z. Li, and X. W. Lou, "General formation of MxCo_{3-x}S₄ (M = Ni, Mn, Zn) hollow tubular structures for hybrid supercapacitors", *Angew. Chem. Int. Ed.*, Vol. 54, No. 36, pp. 10521-10524, 2015.
- [10] K. Chen, F. Liu, D. Xue, and S. Komarneni, "Carbon with ultrahigh capacitance when graphene paper meets K₃Fe(CN)₆", *Nanoscale*, Vol. 7, No. 7, pp. 432-439, 2015.
- [11] S. T. Senthilkumar, R. K. Selvan, and J. S. Melo, "Redox additive/active electrolytes: a novel approach to enhance the performance of supercapacitors", *J. Mater. Chem. A*, Vol. 1, No. 40, pp. 12386-12394, 2013.
- [12] C. Zhao, W. Zheng, X. Wang, H. Zhang, X. Cui, and H. Wang, "Ultrahigh capacitive performance from both Co(OH)₂/graphene electrode and K₃Fe(CN)₆ electrolyte", *Sci. Rep.*, Vol. 3, pp. 2986(1)-2986(6), 2013.
- [13] S. Liu and S. C. Jun, "Hierarchical manganese cobalt sulfide core-shell nanostructures for high-performance asymmetric supercapacitors", *J. Power Sources*, Vol. 342, No. 28, pp. 629-637, 2017.